

Resolving the Structure of Cold Dark Matter Halos

Anatoly Klypin

Astronomy Department, New Mexico State University, Box 30001, Department 4500, Las Cruces, NM 88003-0001

Andrey V. Kravtsov¹, James S. Bullock

Department of Astronomy, The Ohio State University, 140 West 18th Ave., Columbus, OH 43210-1173

Joel R. Primack

Department of Physics, University of California, Santa Cruz, CA 95064

ABSTRACT

We study the effects of mass and force resolution on the density profiles of galaxy-size Cold Dark Matter (CDM) halos in a flat, low-density cosmological model with vacuum energy. We show that although increasing the mass and force resolution allows us to probe deeper into the inner halo regions, it does not lead to steeper inner density profiles. Instead, the halo profiles converge at scales larger than four times the formal resolution or the radius containing more than 200 particles, whichever is larger. In the simulations presented in this paper, we are able to probe density profile of a relaxed isolated galaxy-size halo at scales $r = (0.005 - 1)r_{\text{vir}}$. We find that the density distribution can be well approximated by the profile suggested by Moore et al.(1998): $\rho \propto x^{-1.5}(1 + x^{1.5})^{-1}$, where $x = r/r_s$ and r_s is the characteristic radius. The analytical profile proposed by Navarro et al. (1996) $\rho \propto x^{-1}(1 + x)^{-2}$, also provides a good fit, with the same relative errors of about 10% for radii larger than 1% of the virial radius. Both analytical profiles fit equally well because for high-concentration galaxy-size halos the differences between these profiles become significant only at scales well below $0.01r_{\text{vir}}$. We also find that halos of similar mass may have somewhat different parameters (characteristic radius, maximum rotation velocity, etc.) and shapes of their density profiles. We associate this scatter in properties with differences in halo merger histories and the amount of substructure present in the analyzed halos.

Subject headings: cosmology:theory – galaxy structure – methods: numerical

1. Introduction

During the last decade there has been an increasingly growing interest in testing the predictions of variants of cold dark matter (CDM) models at subgalactic ($\lesssim 100$ kpc) scales. This interest was initiated by indications that observed rotation curves in the central regions of dark matter dominated dwarf galaxies are at odds with predictions

of hierarchical models. Specifically, it was argued (Flores & Primack 1994; Moore 1994) that circular velocities, $v_c(r) \equiv [GM(< r)/r]^{1/2}$, at small galactocentric radii predicted by the models are too high and increase too rapidly with increasing radius compared to the observed rotation curves. The steeper than expected rise of $v_c(r)$ implies that the *shape* of the predicted halo density distribution is incorrect and/or that the DM halos formed in CDM models are too concentrated (i.e., have too much of their mass concentrated in the

¹Hubble Fellow

inner regions).

In addition to the density profiles, there is an alarming mismatch in the predicted abundance of small-mass ($\lesssim 10^8 - 10^9 h^{-1} M_\odot$) galactic satellites and the observed number of satellites in the Local Group (Kauffmann, White & Guiderdoni 1993; Klypin et al. 1999; Moore et al. 1999). Although this discrepancy may well be due to feedback processes (such as photoionization) which prevent gas collapse and star formation in the majority of the small-mass satellites (e.g., Bullock, Kravtsov & Weinberg 2000), the mass scale at which the problem sets in is similar to the scale in the spectrum of primordial fluctuations that may be responsible for the problems with density profiles. In the age of precision cosmology that forthcoming *MAP* and *Planck* cosmic microwave background anisotropy satellite missions are expected to bring, tests of the cosmological models at small scales may prove to be the final frontier and the ultimate challenge to our understanding of cosmology and structure formation in the Universe. However, this obviously requires detailed predictions and checks from the theoretical side, as well as higher resolution/quality observations and a good understanding of their implications and associated caveats. In this paper we focus on the theoretical predictions of the density distribution of DM halos.

A systematic study of halo density profiles for a wide range of halo masses and cosmologies was done by Navarro, Frenk & White (1996, 1997; hereafter NFW), who argued that the analytical profile of the form $\rho(r) = \rho_s(r/r_s)^{-1}(1+r/r_s)^{-2}$ provided a good description of halo profiles in their simulations for all halo masses and in all cosmologies. Here, r_s is the scale radius which, for this profile, corresponds to the scale at which $d \log \rho(r) / d \log r|_{r=r_s} = -2$. The parameters of the profile are determined by the halo's virial mass M_{vir} and *concentration* defined as $c \equiv r_{\text{vir}}/r_s$. NFW argued that there is a tight correlation between c and M_{vir} , which implies that the density distributions of halos of different masses can in fact be described by a one-parameter family of analytical profiles. Further studies by Kravtsov, Klypin & Khokhlov (1997), Kravtsov et al. (1998, hereafter KKBP98), Jing (2000), Bullock et al. (2000), although confirming the $c(M_{\text{vir}})$ correlation, indicated that there is significant scatter in both the

density profiles and concentrations for DM halos of a given mass.

Following the initial studies by Flores & Primack (1994) and Moore (1994), KKBP98 presented a systematic comparison of the results of numerical simulations with rotation curves of a sample of seventeen dark matter dominated dwarf and low surface brightness (LSB) galaxies.

We pointed out that the measured rotation curves of these galaxies all had the same shape with nearly linear central behavior, and furthermore, based on comparison with the density profiles of simulated halos there did not seem to be a significant discrepancy in the *shape* of the density profiles at the scales probed by the numerical simulations ($\gtrsim 0.02 - 0.03 r_{\text{vir}}$, where r_{vir} is halo's virial radius). However, these conclusions were subject to several caveats and required further testing. First, observed galactic rotation curves had to be re-examined more carefully and with higher resolution. The fact that all of the observed rotation curves used in earlier analyses were obtained using relatively low resolution HI observations required checks of the possible beam smearing effects. Also, the possibility of non-circular random motions in the central regions which could modify the rotation velocity of the gas (e.g., Binney & Tremain 1987, p. 198) had to be considered. Second, the theoretical predictions had to be tested for convergence and extended to scales $\lesssim 0.01 r_{\text{vir}}$.

Moore et al. (1998; see also a more recent convergence study by Ghigna et al. 1999) presented a convergence study arguing that mass resolution has a significant impact on the central density distribution of halos. They suggested that at least several million particles per halo are required to reliably model the density profiles at scales $\lesssim 0.01 r_{\text{vir}}$. Based on these results, Moore et al. (1999) advocated a density profile of the form $\rho(r) \propto (r/r_s)^{-1.5}[1 + (r/r_s)^{1.5}]^{-1}$, that behaves similarly ($\rho \propto r^{-3}$) to the NFW profile at large radii, but is steeper at small r : $\rho \propto r^{-1.5}$. Most recently, Jing & Suto (2000) presented a systematic study of density profiles for halo masses in the range $2 \times 10^{12} h^{-1} M_\odot - 5 \times 10^{14} h^{-1} M_\odot$. The study was uniform in mass and force resolution featuring $\sim 5 - 10 \times 10^5$ particles per halo and force resolution of $\approx 0.004 r_{\text{vir}}$. They found that galaxy-mass halos in their simulations are well fit-

ted by the profile² $\rho(r) \propto (r/r_s)^{-1.5} [1 + r/r_s]^{-1.5}$, but that cluster-mass halos are well described by the NFW profile, with logarithmic slope of the density profiles at $r = 0.01r_{\text{vir}}$ changing from ≈ -1.5 for $M_{\text{vir}} \sim 10^{12}h^{-1}\text{M}_{\odot}$ to ≈ -1.1 for $M_{\text{vir}} \sim 5 \times 10^{14}h^{-1}\text{M}_{\odot}$. Jing & Suto interpreted these results as an evidence that profiles of DM halos are not universal (but see §3.1 for a different interpretation).

Rotation curves of a number of dwarf and LSB galaxies have recently been re-examined using H α observations and/or including corrections for beam-smearing in HI observations (e.g., Swaters, Madore & Trewhella 2000; van den Bosch et al. 2000). The results show that for the majority of galaxies, the H α rotation curves are significantly different in their central regions than the rotation curves derived from HI observations. This indicates that the HI rotation curves are affected by beam smearing (Swaters et al. 2000). This also implies that beam smearing may be at least partly responsible for the universal shape of the LSB rotation curves discussed in KKBP98.

It is possible that part of the discrepancy between the rotation curves of the different tracers may be due to real differences in the kinematics of the two gas components (ionized and neutral hydrogen). Preliminary comparisons between the new H α rotation curves and model predictions show that NFW density profiles are consistent with the observed *shapes* of the rotation curves (van den Bosch & Swaters 2000; Navarro & Swaters 2000). Moreover, cuspy density profiles with inner logarithmic slopes as steep as ~ -1.5 also seem to be consistent with the data (van den Bosch & Swaters 2000). A separate concern is not the *shape* of the inner density profile, but rather the value of the central density. There are indications that CDM halos are too concentrated (Navarro & Swaters 2000; McGaugh et al. 2000; Navarro & Steinmetz 2000) in comparison with galactic halos. However, van den Bosch & Swaters (2000) have argued, based on detailed modeling of adiabatic contraction and beam-smearing, that dwarf galaxy concentrations are in fact consistent with

²Note that this profile is somewhat different than the profile advocated by Moore et al., but behaves similarly to the latter at small radii. Figure 9 shows that all three profiles — NFW, Moore, and Jing & Suto — provide good fits to dark matter halos simulated at high resolution.

the observed distribution in Λ CDM halos.

New observational and theoretical developments show that comparison between model predictions and observational data is not straightforward. Decisive comparisons require reaching convergence of theoretical predictions and understanding the kinematics of the gas in the central regions of observed galaxies. In this paper we present convergence tests designed to test effects of mass resolution on the density profiles of halos formed in the currently popular CDM model with cosmological constant (Λ CDM) and simulated using the multiple mass resolution version of the Adaptive Refinement Tree code (ART). We also discuss several caveats with respect to drawing conclusions about the density profiles from the fits of analytical functions to numerical results and their comparisons to observational data. In the following section we describe the code and numerical simulations used in our analysis. In §3 we compare the analytical fits advocated by NFW and Moore et al., fits of these profiles to the density profiles of simulated halos, and convergence analysis of our numerical results.

2. Numerical simulations

2.1. Code description

The Adaptive Refinement Tree code (ART; Kravtsov, Klypin & Khokhlov 1997) was used to run the simulations. The ART code starts with a uniform grid, which covers the whole computational box. This grid defines the lowest (zeroth) level of resolution of the simulation. The standard Particles-Mesh algorithms are used to compute density and gravitational potential on the zeroth-level mesh. The ART code reaches high force resolution by refining all high density regions using an automated refinement algorithm. The refinements are recursive: the refined regions can also be refined, each subsequent refinement having half of the previous level's cell size. This creates a hierarchy of refinement meshes of different resolution, size, and geometry covering regions of interest. Because each individual cubic cell can be refined, the shape of the refinement mesh can be arbitrary and match effectively the geometry of the region of interest.

The criterion for refinement is the local density of particles: if the number of particles in a mesh

cell (as estimated by the Cloud-In-Cell method) exceeds the level n_{thresh} , the cell is split (“refined”) into 8 cells of the next refinement level. The refinement threshold may depend on the refinement level. The code uses the expansion parameter a as the time variable. During the integration, spatial refinement is accompanied by temporal refinement. Namely, each level of refinement, l , is integrated with its own time step $\Delta a_l = \Delta a_0/2^l$, where Δa_0 is the global time step of the zeroth refinement level. This variable time stepping is very important for accuracy of the results. As the force resolution increases, more steps are needed to integrate the trajectories accurately. Extensive tests of the code and comparisons with other numerical N -body codes can be found in Kravtsov (1999) and Knebe et al. (2000).

2.2. Initial conditions

The current version of the ART code has the ability to handle particles of different masses. In the present analysis this ability was used to increase the mass (and correspondingly the force) resolution inside a few pre-selected halos. The multiple mass resolution is implemented in the following way. We set up a realization of the initial spectrum of perturbations in such a way that a very large number of small-mass particles can be generated in the simulation box. For example, for the first (second) set of simulations (see below) we generate 512^3 (1024^3) independent spectrum harmonics. Potentially, initial conditions with $512^3/1024^3$ particles could be generated. Coordinates and velocities of the particles are calculated using all waves ranging from the fundamental mode $k = 2\pi/L$ to the Nyquist frequency $k = 2\pi/L \times N^{1/3}/2$, where L is the box size and N is the number of particles in the simulation.

The code actually generates positions and velocities for all $512^3/1024^3$ particles, but some of the particles are then merged into particles of larger mass. The larger mass (merged) particle is assigned velocity and displacement equal to the average velocity and displacement of the merged particles. The whole lagrangian space of particles is divided into large cubic blocks of particles with each block having 16^3 particles. Depending on what local mass resolution is required, each particular block can be subdivided into smaller sub-blocks and generate from 1 to 16^3 particles (the

highest resolution). Using this procedure³, we can generate particles with 5 different masses covering dynamic mass range of 4096.

We start simulations by making a low resolution run with uniform mass resolution in which all particles have the largest possible mass. Next we run simulations with 32^3 and 64^3 particles. Using these runs, we identify halos in the simulation and select halos to be re-simulated with higher mass and force resolution. For each selected halo we determine its virial radius. We then identify all particles inside the two virial radii and find lagrangian coordinates of each particle. The coordinates are used to mark blocks of particles to generate the initial conditions of the highest mass resolution. Once all particles are processed and all blocks are marked, we mark all blocks adjacent to those already marked to produce initial conditions of the eight times lower mass resolution. This procedure is repeated for lower and lower mass resolution levels. In the end, each unmarked block will produce one most massive particle and a marked block will generate a number of particles which depends on the step in which the block was marked. Figure 1 shows the outcome of the process of mass refinement in a 2-dimensional case.

Figure 2 shows an example of mass refinement for one of the halos in our simulations. A large fraction of high resolution particles ends up in the central halo, which does not have any larger mass particles (see insert in the bottom panel). At $z = 10$, the region occupied by the high resolution particles is non-spherical: it is substantially elongated in the direction perpendicular to the large filament clearly seen at $z = 0$.

After the initial conditions are set, we run the simulation again allowing the code to perform mesh refinement based only on the number of particles with the smallest mass.

2.3. Numerical simulations

We simulated a flat low-density cosmological model (Λ CDM) with $\Omega_0 = 1 - \Omega_\Lambda = 0.3$, the Hubble parameter (in units of $100 \text{ kms}^{-1}\text{Mpc}^{-1}$) $h = 0.7$, and the spectrum normalization $\sigma_8 = 0.9$. We have run two sets of simulations. The first set

³The code is actually written to handle an arbitrary dynamic range. The current limit is determined by computational limitations.

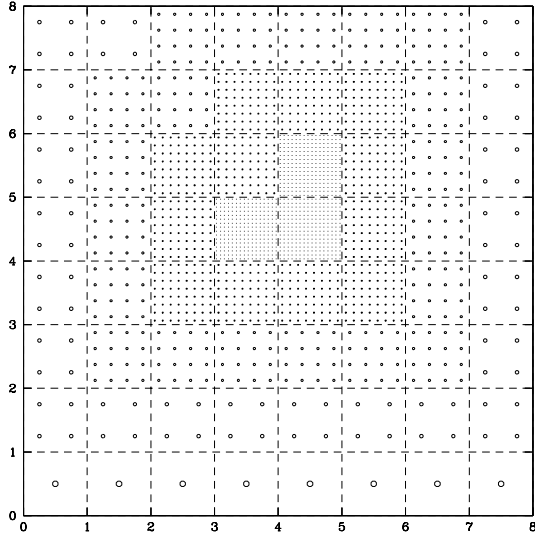


Fig. 1.— Example of the construction of mass refinement in lagrangian space (here for illustration we show a 2D case). Three central blocks of particles were marked for highest mass resolution. Each block produces 16^2 particles of the smallest mass. Adjacent blocks correspond to the four times lower resolution and produce 8^2 particles each. The procedure is repeated recursively until we reach the lowest level of resolution. The region of the highest resolution can have arbitrary shape.

used 128^3 zeroth-level grid in a computational box of $30h^{-1}\text{Mpc}$. These simulations were run to the present moment $z = 0$. The second set of simulations used 256^3 grid in a $25h^{-1}\text{Mpc}$ box. These simulations had higher mass resolution and therefore produced more halos but were run only to $z = 1$. In the simulations used in this paper, the threshold for cell refinement (see above) was low on the zeroth level: $n_{\text{thresh}}(0) = 2$. Thus, every zeroth-level cell containing two or more particles was refined. This was done to preserve all small-scale perturbations present in the initial spectrum of perturbations. The threshold was higher on deeper levels of refinement. For the first set of simulations it was $n_{\text{thresh}} = 2$ at the first refinement level and $n_{\text{thresh}} = 3$ for all higher levels. For the second simulation the thresholds were $n_{\text{thresh}} = 3$ and $n_{\text{thresh}} = 4$ for the first level and higher levels, respectively.

In all of our simulations, the step in the expansion

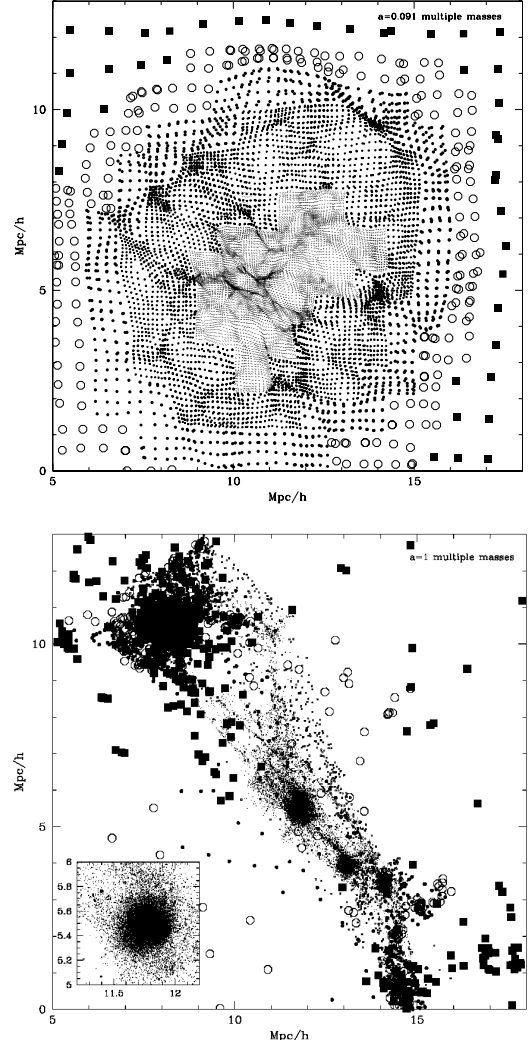


Fig. 2.— Distribution of particles of different masses in a thin slice through the center of halo A_1 (see Table 1) at $z = 10$ (top panel) and at $z = 0$ (bottom panel). To avoid crowding of points the thickness of the slice is made smaller in the center (about $30h^{-1}\text{kpc}$) and larger ($1h^{-1}\text{Mpc}$) in the outer parts of the forming halo. Particles of different mass are shown with different symbols: tiny dots, dots, large dots, and open circles.

parameter was chosen to be $\Delta a_0 = 2 \times 10^{-3}$ on the zero level of resolution. This gives about 500 steps for particles located in the zeroth level for an entire run to $z = 0$. We have done a test run with twice smaller time step for a halo of mass comparable (but with smaller number of particles)

to the mass of halos studied in this paper. We did not find any significant differences in the resulting halo profile. In the first set of simulations, the highest level of refinement was ten, which corresponds to $500 \times 2^{10} \approx 500,000$ time steps at the tenth refinement level. For the second set of simulations, nine levels of refinement were reached which corresponds to 128,000 steps at the highest refinement level.

In the following sections we present density profiles of four halos. The first halo (*A*) was the only halo selected for re-simulation in the first set of simulations. In this case, the selected halo was relatively quiescent at $z = 0$ and had no massive neighbors. The halo was located in a long filament bordering a large void and was about 10 Mpc away from the nearest cluster-size halo. After the high-resolution simulation was completed we found that the nearest galaxy-size halo was about 5 Mpc away. The halo had a fairly typical merging history with $M(t)$ track slightly lower than the average mass growth predicted using the extended Press-Schechter model. The last major merger event occurred at $z \approx 2.5$; at lower redshifts the mass growth (the mass in this time interval has grown by a factor of three) was due to slow and steady mass accretion.

The second set of simulations was performed in a different manner. In the low resolution run we selected three halos (B, C, and D) residing in a well pronounced filament. Two of the halos are neighbors located about 0.5 Mpc from each other. The third halo was 2 Mpc away from this pair. Thus, the halos were not selected to be too isolated as was the case in the first set of runs. Moreover, the simulation was analyzed at an earlier moment ($z = 1$) where halos are more likely to be unrelaxed. Therefore, we consider the halo *A* from the first set as an example of a rather isolated well-relaxed halo. In many respects, this halo is similar to halos simulated by other research groups that used multiple mass resolution techniques. The three halos from the second set of simulations can be viewed as representative of more typical halos: located in more crowded environments and not necessarily well relaxed.

Parameters of the simulated dark matter halos are listed in Table 1. Columns in the table present (1) Halo “name” (halos A₁, A₂, A₃ are the halo A re-simulated three times with different

mass and force resolutions); (2) redshift at which the halo was analyzed; (3-5) virial mass, comoving virial radius, and maximum circular velocity. At $z = 0$ ($z = 1$) the virial radius was estimated as the radius within which the average over-density of matter is 340 (180) times larger than the mean cosmological density of matter at that redshift; (6) the number of particles within the virial radius; (7) the smallest particle mass in the simulation; (8) formal force resolution achieved in the simulation (as we will show below, convergent results are expected at scales larger than four times the formal resolution); (9) halo concentration as estimated from NFW profile fits to halo density profiles; (10) maximum relative error of the NFW fit: $\rho_{\text{NFW}}/\rho_{\text{halo}} - 1$ (the error was estimated inside $50h^{-1}\text{kpc}$ radius); (11) the same as in the previous column, but for the fits of the profile advocated by Moore et al.

3. Results

3.1. Comparison of the NFW and the Moore et al. profiles

Before we fit analytical profiles to profiles of simulated dark matter halos or compare them to the observed rotation curves, it is instructive to compare different analytical approximations. Although the NFW and Moore et al. profiles predict different behavior of $\rho(r)$ in the central regions of a halo, the scale at which this difference becomes significant depends on the specific values of the halo’s characteristic density and radius. Table 2 presents the parameters and statistics associated with the two analytical profiles. For the NFW profile more information can be found in Klypin et al. (1998), Łokas & Mamon (2000), and Widrow (2000).

Each profile is defined by two independent parameters. We choose these to be the characteristic density ρ_s and radius r_s . In this case all expressions describing the properties of the profiles have a simple form and do not depend on the concentration. Both the concentration and the virial mass appear only in the normalization of the expressions. The choice of the virial radius (e.g., Łokas & Mamon 2000) as a scale unit results in more complicated expressions with explicit dependence on the concentration. In this case, one has to be careful about the definition of the virial radius, as

TABLE 1
PARAMETERS OF HALOS

Name	z	M_{vir} $h^{-1}M_{\odot}$	R_{vir} $h^{-1}\text{kpc}$	V_{max} km/s	N_{part}	m_{part} $h^{-1}M_{\odot}$	FormRes	C_{NFW}	RelErr	RelErr
(1)	(2)	(3)	(4)	(5)	(6)	(7)	$h^{-1}\text{kpc}$	(9)	NFW	Moore
A ₁	0	1.97×10^{12}	257	247.0	1.2×10^5	1.6×10^7	0.23	17.4	0.17	0.20
A ₂	0	2.05×10^{12}	261	248.5	1.5×10^4	1.3×10^8	0.91	16.0	0.13	0.16
A ₃	0	1.98×10^{12}	256	250.5	1.9×10^3	1.1×10^9	3.66	16.6	0.16	0.10
B	1	8.5×10^{11}	241	195.4	7.1×10^5	1.2×10^6	0.19	12.3	0.23	0.16
C	1	6.8×10^{11}	208	165.7	5.0×10^5	1.2×10^6	0.19	11.9	0.37	0.20
D	1	9.6×10^{11}	245	202.4	7.9×10^5	1.2×10^6	0.19	9.5	0.25	0.60

there are several definitions in the literature. For example, it is often defined as the radius, r_{200} , within which the average density is 200 times the *critical density*. In this paper the virial radius is defined as the radius within which the average density is equal to the density predicted by the top-hat model: it is δ_{TH} times the *average matter density* in the Universe. For the $\Omega_0 = 1$ case these two definitions are equivalent. In the case of $\Omega_0 = 0.3$ models, however, the virial radius is about 30% larger than r_{200} (e.g., Eke et al. 1998).

There is no unique way of defining a consistent concentration for the different analytical profiles. Again, it is natural to use the characteristic radius r_s to define the concentration: $c \equiv r_{\text{vir}}/r_s$. This simplifies the expressions. At the same time, if we fit the dark matter halo with the two profiles, we will get different concentrations because the values of the corresponding r_s will be different. Alternatively, if we choose to match the outer regions of the profiles (say, $r > r_s$) as closely as possible, we may choose to change the ratio of the characteristic radii $r_{s,\text{NFW}}/r_{s,\text{Moore}}$ in such a way that both profiles reach the maximum circular velocity v_{circ} at the same physical radius r_{max} . In this case, the formal concentration of the Moore et al. profile is 1.72 times smaller than that of the NFW profile. Indeed, with this normalization profiles look very similar in the outer parts as one finds in Figure 3. Table 2 also gives two other “concentrations”. The concentration $C_{1/5}$ is defined as the ratio of virial radius to the radius, which encompasses 1/5 of the virial mass (Avila-Reese et al. 1999). For

halos with $C_{\text{NFW}} \approx 5.5$ this 1/5 mass concentration is equal to C_{NFW} . One can also define the concentration as the ratio of the virial radius to the radius at which the logarithmic slope of the density profile is equal to -2 . This scale corresponds to r_s for the NFW profile and $\approx 0.35r_s$ for the Moore et al. profile.

Figure 3 presents the comparison between the analytic profiles normalized to have the same virial mass and the same radius r_{max} . We show results for halos of low and high values of concentration representative of cluster- and low-mass galaxy halos, respectively. The bottom panels show the profiles, while the top panels show the corresponding logarithmic slope as a function of radius. The figure shows that the two profiles are very similar throughout the main body of the halos. Only in the very central region do the differences become significant. The difference is more apparent in the logarithmic slope than in the actual density profiles. Moreover, for galaxy-mass halos the difference sets in at a rather small radius $\lesssim 0.01r_{\text{vir}}$, which would correspond to scales < 1 kpc for the typical dark matter dominated dwarf and LSB galaxies. In most analyses involving galaxy-size halos, the differences between NFW and Moore et al. profiles are irrelevant, and the NFW profile provides an accurate description of the density distribution.

Note also that for galaxy-size (e.g., high-concentration) halos the logarithmic slope of the NFW profile has not yet reached its asymptotic inner value of -1 even at scales as small as $0.01r_{\text{vir}}$.

TABLE 2
COMPARISON OF NFW AND MOORE ET AL. PROFILES

Parameter	NFW	Moore et al.
Density $x = r/r_s$	$\rho = \frac{\rho_s}{x(1+x)^2}$ $\rho \propto x^{-3}$ for $x \gg 1$ $\rho \propto x^{-1}$ for $x \ll 1$ $\rho/\rho_s = 1/4$ at $x = 1$	$\rho = \frac{\rho_s}{x^{1.5}(1+x)^{1.5}}$ $\rho \propto x^{-3}$ for $x \gg 1$ $\rho \propto x^{-1.5}$ for $x \ll 1$ $\rho/\rho_s = 1/2$ at $x = 1$
Mass $M = 4\pi\rho_s r_s^3 f(x)$ $= M_{\text{vir}} f(x)/f(C)$ $M_{\text{vir}} = \frac{4\pi}{3} \rho_{\text{cr}} \Omega_0 \delta_{\text{top-hat}} r_{\text{vir}}^3$	$f(x) = \ln(1+x) - \frac{x}{1+x}$	$f(x) = \frac{2}{3} \ln(1+x^{3/2})$
Concentration $C = r_{\text{vir}}/r_s$	$C_{\text{NFW}} = 1.72 C_{\text{Moore}}$ for halos with the same M_{vir} and r_{max} $C_{1/5} \approx \frac{C_{\text{NFW}}}{0.86 f(C_{\text{NFW}}) + 0.1363}$ error less than 3% for $C_{\text{NFW}} = 5-30$ $C_{\gamma=-2} = C_{\text{NFW}}$	$C_{\text{Moore}} = C_{\text{NFW}}/1.72$ $C_{1/5} = \frac{C_{\text{Moore}}}{[(1+C_{\text{Moore}}^{3/2})^{1/5} - 1]^{2/3}}$ $\approx \frac{C_{\text{Moore}}}{[C_{\text{Moore}}^{3/10} - 1]^{2/3}}$ $C_{\gamma=-2} = 2^{3/2} C_{\text{Moore}}$ $\approx 2.83 C_{\text{Moore}}$
Circular Velocity $v_{\text{circ}}^2 = \frac{GM_{\text{vir}}}{r_{\text{vir}}} \frac{C}{x} \frac{f(x)}{f(C)}$ $= v_{\text{max}}^2 \frac{x_{\text{max}}}{x} \frac{f(x)}{f(x_{\text{max}})}$ $v_{\text{vir}}^2 = \frac{GM_{\text{vir}}}{r_{\text{vir}}}$	$x_{\text{max}} \approx 2.15$ $v_{\text{max}}^2 \approx 0.216 v_{\text{vir}}^2 \frac{C}{f(C)}$ $\rho/\rho_s \approx 1/21.3$ at $x = 2.15$	$x_{\text{max}} \approx 1.25$ $v_{\text{max}}^2 \approx 0.466 v_{\text{vir}}^2 \frac{C}{f(C)}$ $\rho/\rho_s \approx 1/3.35$ at $x = 1.25$

Figure 4 shows the logarithmic slope of the NFW profile at scales $\approx 0.01 - 0.02r_{\text{vir}}$ as a function of halo virial mass for the Λ CDM model studied here. The average $c_{\text{vir}}(M)$ for this model given in Bullock et al. (2000) is used here. For $\sim 10^{12}h^{-1}\text{M}_{\odot}$ halos the logarithmic slope of the NFW profile is $\approx -1.4 - 1.5$, while for cluster-size halos this slope is ≈ -1.2 . This dependence of the slope at a given fraction of the virial radius on the virial mass of the halo is very similar to the results plotted in Figure 3 of Jing & Suto (2000). These authors interpreted it as evidence that halo profiles are not universal. It is obvious, however, that their results are consistent with NFW profiles and the dependence of the slope on mass can be simply a manifestation of the well-studied $c_{\text{vir}}(M)$ relation.

In Figure 5 we compare the NFW and Moore et al. profiles in a different way. We approximate the Moore et al. halo of a given concentration with the NFW profile. Fractional deviations of the fits are shown in the figure for halos of different concentration and for three ranges of radii used for the fits: $0.003, 0.01, 0.02 < r/r_{\text{vir}} < 1$. The low-concentration halo has larger deviations, but even in this case, the deviations are less than 15% if we fit the halo at scales $0.01 < r/r_{\text{vir}} < 1$. For the high-concentration halo, the deviations are much smaller: less than 8% when the NFW profile is fit in the same range of scales.

To summarize, we find that the differences between the NFW and the Moore et al. profiles are very small ($\Delta\rho/\rho < 10\%$) for radii above 1% of the virial radius for typical galaxy-size halos with $C_{\text{NFW}} \gtrsim 12$. The differences are larger for halos with smaller concentrations. In the case of the NFW profile, the asymptotic value of the central slope $\gamma = -1$ is not achieved even at radii as small as 1%-2% of the virial radius.

3.2. Convergence study

Halo A in the first set of simulations was resimulated three times with increasing mass resolution. For each simulation, we considered outputs at four time moments in the interval $z = 0 - 0.03$. Parameters of the halos in these simulations averaged over the four moments are presented in the first three rows of the Table 1. Results presented in the Table show that there are no systematic changes with resolution in the values of

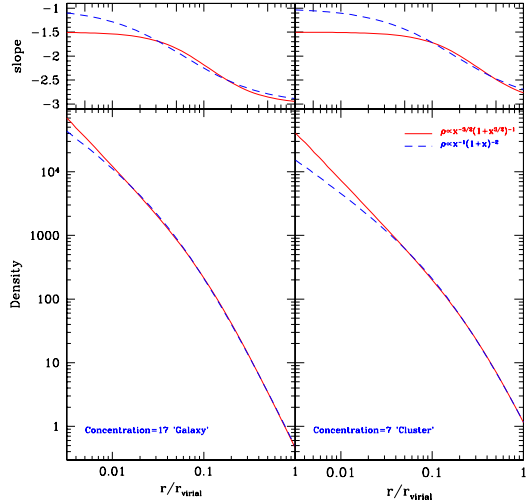


Fig. 3.— Comparison of the Moore et al. and the NFW profiles. Each profile is normalized to have the same virial mass and the same radius of the maximum circular velocity. *Left panels*: High-concentration halo typical of small galaxy-size halos $C_{\text{NFW}} = 17$. *Right panels*: Low-concentration halo typical of cluster-size halos. The deviations are very small (< 3%) for radii $r > r_s/2$. Top panels show the local logarithmic slope of the profiles. Note that for the high concentration halo the slope of the profile is significantly larger than the asymptotic value -1 even at very small radii $r \approx 0.01/r_{\text{vir}}$.

halo parameters both on the virial radius scale and around the maximum of the circular velocity ($r = 30 - 40h^{-1}\text{kpc}$).

Figure 6 shows the central region of the halo A_1 (see Table 1). This figure is similar to the Fig.1a in Moore et al. (1998) in that all profiles are drawn to the formal force resolution and the straight lines indicate slopes of two power-laws $-\gamma = -1$ and $-\gamma = -1.4$. At the first glance, it may seem that the NFW profile is not a good fit because at around 1% of the virial radius the slope is steeper than -1 and because the central slope increases as we increase the mass resolution. Indeed, Moore et al. (1998) interpreted their Fig.1a in this way. We argue that both conclusions are not correct because the simulated profiles are considered at scales beyond the range where convergence is achieved. We also note that the results of our highest resolution

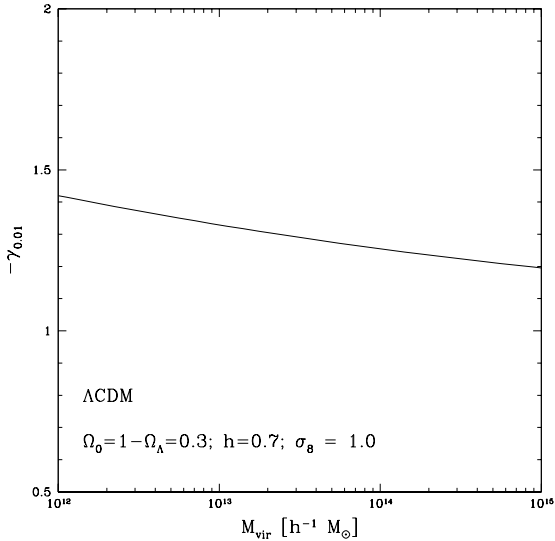


Fig. 4.— Logarithmic slope at the scale $0.01 - 0.02r_{\text{vir}}$ for the NFW profile as a function of halo virial mass. The ΛCDM cosmology and $C_{\text{vir}}(M)$ appropriate for this model at $z = 0$ (see Bullock et al. 2000) are assumed to compute $\gamma_{0.01}$.

run A_1 are qualitatively consistent with results of Kravtsov et al. (1998). Indeed, if the profiles are considered down to the scale of *two* formal resolutions (a scale smaller than the smallest converged scale), the density profile slope in the very central part of the profile $r \lesssim 0.01r_{\text{vir}}$ is close to $\gamma = -0.5$.

The profiles in Figure 6 reflect the density distribution in the cores of simulated halos. However, this density distribution is affected by numerical effects. Indeed, the profiles in Figure 6 are shown below actual resolution. The formal resolution usually does not even correspond to the scale where the numerical force is fully Newtonian (usually it is still considerably “softer” than the Newtonian value). In the ART code, the interparticle force reaches (on average) the Newtonian value at about two formal resolutions (see Kravtsov et al. 1997). It is clear, therefore, than in order to draw conclusions about density distribution we need to determine the range of scales at which convergence was reached.

The effects of force resolution can be studied by resimulating the same objects with higher force resolution and comparing the density profiles. Such a convergence study was done in

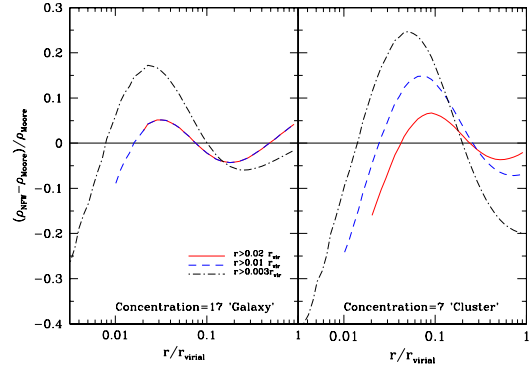


Fig. 5.— Density deviations of the halos profiles. A halo with the Moore et al. profile was approximated by the NFW profile. Different ranges of radii were used to make the fit as indicated in the plot. *Left panel:* High concentration $C_{\text{NFW}} = 17$ halo. *Right panel:* Low concentration $C_{\text{NFW}} = 7$ halo.

Kravtsov et al. (1998) where it was found that *for a fixed mass resolution*, halo density profiles converge at scales above two formal resolutions. However, one also should consider integration errors of particle trajectories. They mostly affect the innermost highest-density regions of halos, close to the the limit of force resolution. The local dynamical time for particles moving in the core of a halo is very short. For example, particles on a circular orbit of radius $1h^{-1}\text{kpc}$ from the center of halo A makes about 200 revolutions over the Hubble time. Therefore, if the time step is not sufficiently small, numerical errors in these regions will tend to grow. Even for small time steps errors exist and tend to alter the density distribution in the centers of halos. Another possible source of numerical errors is mass resolution. For example, poor mass resolution in simulations with good force resolution may lead to two-body effects (e.g., Knebe et al. 2000). An insufficient number of particles may also result in a “grainy” potential in halo cores and thereby affect accuracy of orbit integration. In these effects, mass and force resolution may be closely related.

Thus, it is clear that in order to make conclusions not affected by numerical errors, one has to determine the range of trustworthy scales using convergence analysis. Figure 7 shows that for the halo A, convergence for vastly different mass and force resolutions is reached for scales $\gtrsim 4$ formal force resolutions (all profiles in this figure are plotted down to the radius of 4 formal force resolutions). For all resolutions, there are more than 200 particles within the radius of four resolutions from the halo center. For the highest resolution simulation (halo A₁) convergence is reached at scales $\gtrsim 0.005r_{\text{vir}}$, assuming convergence at 4 times the formal resolution as for halos A₂ and A₃.

In order to judge which analytical profile provides a better description of the simulated profiles we fitted the NFW and Moore et al. analytic profiles. Figure 8 presents results of the fits and shows that both profiles fit the simulated profile equally well: fractional deviations of the fitted profiles from the numerical one are smaller than 20% over almost three decades in radius. It is thus clear that the fact that the numerical profile has slope steeper than -1 at the scale of $\sim 0.01r_{\text{vir}}$ does not mean that good fit of the NFW profile (or even analytic profiles with shallower asymptotic slopes) cannot be obtained.

There is definitely a certain degree of degeneracy in fitting various analytic profiles to numerical results. Figure 9 illustrates this further by showing results of fitting profiles (solid lines) of the form $\rho(r) \propto (r/r_0)^{-\gamma} [1 + (r/r_0)^\alpha]^{-(\beta-\alpha)/\gamma}$ to the same simulated halo profile (halo A₁) shown as solid circles. The legend in each panel indicates the corresponding values of α , β , and γ of the fit; the digit in parenthesis indicates whether the parameter was kept fixed (0) or not (1) during the fit. The two right panels show fits of the NFW and Moore et al. profile; the bottom left panel shows fit of the profiles used by Jing & Suto (2000). The top left panel shows a fit in which the inner slope was fixed but α and β were fit. The figure shows that all four analytic profiles can provide a good fit to the numerical profile in the whole range of resolved scales: $0.005 - 1r_{\text{vir}}$.

3.3. Halo profiles at $z = 1$

As we mentioned in § 2.3, the halo A analyzed in the previous section is somewhat special because it was selected as an isolated relaxed halo.

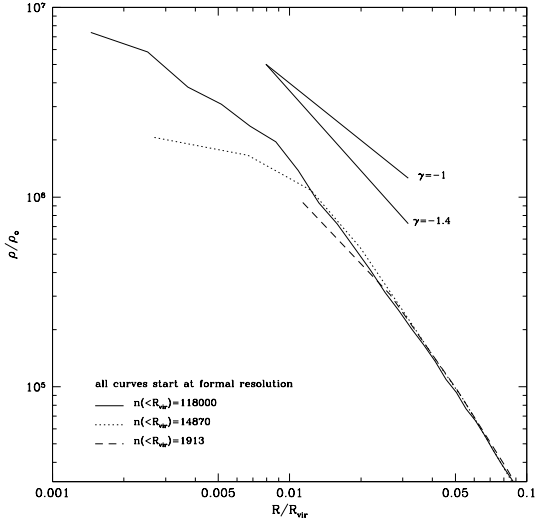


Fig. 6.— Density profiles of halo A simulated with different mass and force resolutions. The profiles are plotted down to the formal force resolution of each simulation. Because the plot shows results below the actual force resolution, one gets a wrong impression that the profile gets steeper and the concentration increases when the mass resolution is increased.

In order to reach unbiased conclusions, in this section we will present analysis of halos from the second set of simulations (halos B, C, and D in Table 1) which were not selected to be relaxed or isolated. Based on the results of the convergence study presented in the previous section, we will consider profiles of these halos only at scales above four formal resolutions and not less than 200 particles. Note that these conditions are probably more stringent than necessary because these halos were simulated with 5 – 7 times more particles per halo than halo A₁. There is an advantage in analyzing halos at a relatively high redshift. Halos of a given mass will have lower concentration (see Bullock et al. 2000). Lower concentration implies a large scale at which the asymptotic inner slope is reached. Profiles of the high redshift halos should therefore be more useful in discriminating between the analytic models with different inner slopes.

We found that substantial substructure is present inside the virial radius in all three halos. Figure 10 shows profiles of these halos at $z = 1$. These profiles are not as smooth as that

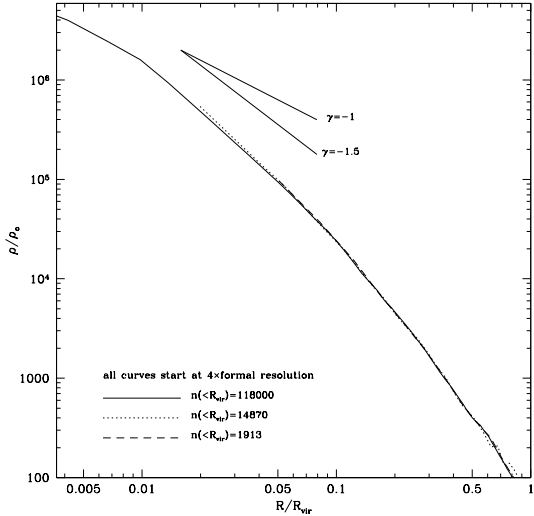


Fig. 7.— The same as in Figure 6 but with the profiles plotted down to *four* formal resolutions. It is clear that for vastly different mass (from 2000 to 120000 particles in the halo) and force (from $3.66h^{-1}$ kpc to $0.23h^{-1}$ kpc) resolutions the convergence is reached at these scales. At the scale of a few percent of the virial radius the density profile is visibly steeper than the limiting slope $\gamma = -1$ of the NFW profile. However, this is due to the high concentration of the halo and should not be interpreted as a failure of the NFW profile.

of halo A₁ due to the substructure. Note that bumps and depressions visible in the profiles have amplitude that is significantly larger than the shot noise. Halo C appeared to be the most relaxed of the three halos. This halo had its last major merger somewhat earlier than the other two. Halo D had a major merger event at $z \approx 2$. A remnant of the merger is still visible as a bump at $r \sim 100h^{-1}$ kpc. The non-uniformities of profiles caused by substructure may substantially bias analytic fits if one uses the entire range of scales below the virial radius. Therefore, we used only the central, presumably more relaxed, regions in the analytic fits: $r < 50h^{-1}$ kpc for halo D and $r < 100h^{-1}$ kpc for halos B and C (fits using only central $50h^{-1}$ kpc did not change results).

The best fit parameters were obtained by minimizing the maximum fractional deviation of the fit: $\max[\text{abs}(\log \rho_{\text{fit}} - \log \rho_{\text{halo}})]$. Minimizing the sum of squares of deviations (χ^2), as is often done,

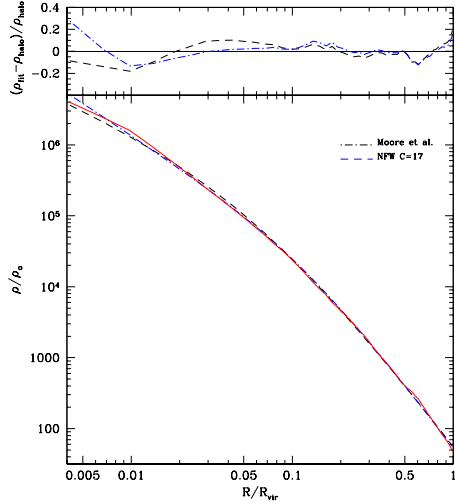


Fig. 8.— Fits of the NFW and Moore et al. halo profiles to the profile of halo A₁ (*bottom panel*). The *top panel* shows fractional deviations of the analytic fits from the numerical profile. Note that both analytic profiles fit numerical profile equally well: fractional deviations are smaller than 20% over almost three decades in radius.

can result in larger errors at small radii with the false impression that the fit fails because it has a wrong central slope. The fit that minimizes maximum deviations improves the NFW fit for points in the range of radii $(5 - 20)h^{-1}$ kpc, where the NFW fit would appear to be below the data points if the fit was done by the χ^2 minimization. For example, if we fit halo B by minimizing χ^2 , the concentration slightly decreases from 12.3 (see Table 1) to 11.8, the maximum error slightly increases to 27%, but the fit goes below the data points for most of the points at small radii.

We also made a fit for halo B assuming even more stringent limits on the effects of numerical resolution. We fitted the halo starting at the scale equal to six times the formal resolution, minimizing the maximum deviation. Inside this radius there were about 900 particles. Resulting parameters of the fit were close to those in Table 1: $C_{\text{NFW}} = 11.8$, and maximum error of the NFW fit was 17%.

We found that for halos B and C the errors in the Moore et al. fits were systematically smaller

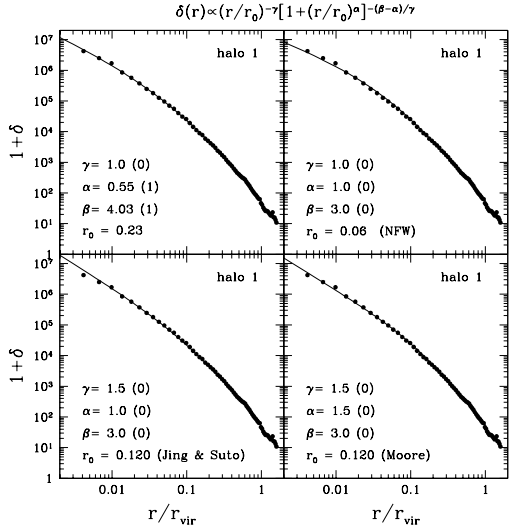


Fig. 9.— Analytic fits to the density profile of the halo A_1 from our set of simulations. The fits are of the form $\rho(r) \propto (r/r_0)^{-\gamma}[1 + (r/r_0)^\alpha]^{-(\beta-\alpha)/\gamma}$. The legend in each panel indicates the corresponding values of α , β , and γ of the fit; the digit in parenthesis indicates whether the parameter was kept fixed (0) or not (1) during the fit. Note that various sets of parameters α , β , γ provide equally good fits to the simulated halo profile in the whole range resolved range of scales $\approx 0.005 - 1r_{\text{vir}}$. This indicates a large degree of degeneracy in parameters α , β , and γ .

than those of the NFW fits, though the differences were not dramatic. But the Moore et al. fit failed for halo D . It formally gave very small errors, but this was done for a fit with unreasonably small concentration $C = 2$. When we constrained the approximation to have about twice larger concentration as compared with the best NFW fit, we were able to obtain a reasonable fit (this fit is shown in Figure 10). Nevertheless, the central part was fit poorly in this case.

Therefore, our analysis does not show that one analytic profile is better than the other for description of the density distribution in simulated halos. Despite the larger number of particles per halo and the lower concentrations of $z = 1$ halos, results are still inconclusive. The Moore et al. profile is a better fit to the profile of halo C ; the NFW profile is a better fit to the central part of the halo D . Halo B represents an intermediate case where

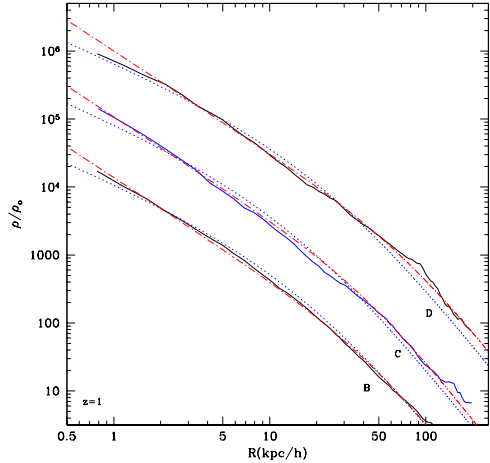


Fig. 10.— Profiles of halos B, C, D (see Table 1) at $z = 1$. Profiles of halos C and D were offset downwards by factors of 10 and 100 for clarity. *Solid curves* show simulated profiles, while *dotted and dot-dashed curves* show the NFW and Moore et al. fits, respectively. The halo profiles in simulations are plotted down to four times the formal resolution. Each halo had more than 200 particles inside the smallest plotted scale.

both profiles provide equally good fits (similar to the analysis of halo A).

Note that there seem to be real deviations in parameters of halos of the same mass. Halos B and D have the same virial radii and nearly the same circular velocities, yet their concentrations are different by 30%. We find the same differences in estimates of $C_{1/5}$ concentrations, which do not depend on specifics of an analytic fit. The central slope at around 1kpc also changes from halo to halo.

4. Discussion and conclusions

We have analyzed a series of simulations with vastly different mass and force resolution with the goal of studying density distribution in the central regions of galaxy-size dark matter halos. We used multiple mass simulations performed using the ART code; the simulations were done with variable mass, force and temporal resolutions. In the highest resolution runs, we achieved a (formal)

spatial dynamical range of $2^{17} = 131,072$; the simulation was run with 500,000 steps for particles at the highest level of refinement.

Using these simulations, we have studied convergence of halo density profiles for different mass and force resolutions. Our conclusions regarding the convergence of the profiles differ from those of Moore et al. (1997). Unlike Moore et al. (1997), we *do not* find that the inner slope increases with increasing mass resolution, or that halos become more concentrated. We show that the halo profiles converge at scales larger than a certain (true numerical resolution) scale defined by numerical effects. This scale is probably code dependent, but can be found for any numerical code by a convergence study. For the ART simulations presented here, the density profiles converged at the scale of four times the formal force resolution or the radius containing more than 200 particles, whichever is larger. Our results are consistent with results of the “Santa Barbara” cluster comparison project (Frenk et al. 1999): at a fixed *resolved* scale results do not change as the resolution increases.

We can reproduce results of Moore et al. (1998) and results of KKP98 regarding shallow central profiles, but only when we consider scales below the true resolution. For example, if we plot halo density profiles down to the formal resolution of the simulation, as in Moore et al. (1998), we indeed find that density profiles do not converge in the innermost region of the halo.

In KKP98 we have discussed convergence tests in which we varied force resolution while keeping mass resolution fixed. Using these tests we concluded that density profiles converge at radii twice the formal peak resolution of a simulation. The convergence tests presented in this paper, however, show that mass resolution places more stringent conditions on the trustworthy range of scales. Although we can reproduce our previous results (shallow than -1 density profiles at radii of two formal resolution), our new convergence tests show that these results were affected by limited mass resolution. We conclude that we overestimated our force resolution KKP98 and that the shallow central slopes presented there were an artifact of that overestimate. However, all of the results presented KKP98 focusing on general halo characteristics, such as the scatter in profile shapes, and the agreement between the V_{max} —

r_{max} relations of simulated dark halos and dark matter dominated dwarf and LSB galaxies, are valid. At scales above four times the formal resolution and containing more than 200 particles results presented in this paper agree well with previous simulations. For example, the concentration parameter for the halo A is consistent with the $c(M)$ relation found in Bullock et al. (2000) based on the previous simulations. The concentrations for halos B, C, D are also in good agreement with the concentration evolution found in Bullock et al.

We show that for the galaxy-size halos considered in this paper ($M_{vir} = 7 \times 10^{11} h^{-1} M_{\odot} - 2 \times 10^{12} h^{-1} M_{\odot}$ and $C = 9 - 17$) both the NFW profile $\rho \propto r^{-1}(1+r)^{-2}$ and the Moore et al. profile $\rho \propto r^{-1.5}(1+r^{1.5})^{-1}$ give good fits with accuracy about 10% for radii larger than 1% of the virial radius. Both profiles provide an equally good fit. For dwarf and LSB galaxies commonly used for comparisons with model predictions, this corresponds to scales $\gtrsim 1$ kpc. Therefore, the debate about which analytic profile provides a better description of the CDM halo profiles may well be irrelevant for comparisons to measured galaxy rotation curves. Such comparisons are also subject to other uncertainties, one of which is the limited spatial extent of the observed rotation curves. The particular shape of the inner density distribution may be important for galaxy cluster observations, however. Cluster-size halos are predicted to have smaller concentrations, which means that the scale at which differences between the NFW and Moore et al. profiles become significant is larger and is observationally relevant.

We show that density profiles of halos that are not fully relaxed may contain real non-uniformities due to substructure and differences in the density distributions. These non-uniformities lead to different best fit functional forms and to different values of fitted parameters (e.g., concentration). For example, we found that the profile of halo C in our second set of simulations is best fit by the Moore et al. profile. The density profile of halo D, however, is best fit by the NFW profile, while that of halo B is fit equally well by the NFW and Moore et al. profiles. Note that these three halos were simulated with the same mass and force resolution. The main difference between them is their different merger histories. We conclude, therefore,

that differences in merger history and different degree of substructure in halos of the same mass may explain the scatter in profile shapes and concentration parameters found in previous studies (KKBP98; Jing 2000; Bullock et al. 2000).

In summary, the study presented here is aimed to clarify the issue of convergence of the inner density profiles of CDM halos. We show that convergence can be reached regardless of the mass resolution. Our results also indicate that there is a real scatter in shapes of density profiles and halo parameters. Larger systematic studies may put these conclusions on a firmer footing.

We acknowledge support from the grants NAG-5- 3842 and NST- 9802787, and also NASA and NSF grants at UCSC. A.V.K. acknowledges support by NASA through Hubble Fellowship grant HF-01121.01-99A from the Space Telescope Science Institute, which is operated by the Association of Universities for Research in Astronomy, Inc., under NASA contract NAS5-26555. JSB was supported by NASA LTSA grant NAG5-3525 and NSF grant AST-9802568. JRP acknowledges a Humboldt Award. Computer simulations presented in this paper were done at the National Center for Supercomputing Applications (NCSA), Urbana-Champaign, Illinois.

REFERENCES

Binney, J., & Tremaine, S. 1987, *Galactic Dynamics*, Princeton: Princeton Univ. Press

Bullock, J.S., Kolatt, T.S., Sigad, Y., Somerville, R.S., Kravtsov, A.V., Klypin, A., Primack, J.P., Dekel, A. 2000, MNRAS submitted (astro-ph/9908159)

Bullock, J.S., Kravtsov, A.V., & Weinberg, D.H. 2000, ApJ in press (astro-ph/0002214)

Eke, V.R., Cole, S., Frenk, C.S., & Henry, P.J. 1998, MNRAS, 298, 1145

Flores, R.A., & Primack, J.R. 1994, ApJ 427, L1

Frenk, C.S. et al. 1999, ApJ, 525, 554

Ghigna, S., Moore, B., Governato, F., Lake, G., Quinn, T., Stadel, J. 1999, ApJ submitted (astro-ph/9910166)

Jing, Y.P. 2000, ApJ, 535, 30

Jing, Y.P. & Suto, Y. 2000, ApJ 529, L69

Kauffmann, G., White, S.D.M., & Guiderdoni, B. 1993, MNRAS 264, 201

Klypin, A., Gottlöber, S., Kravtsov, A.V., Khokhlov, A. 1998, ApJ, 516, 530

Klypin, A., Kravtsov, A.V., Valenzuela, O., & Prada, F. 1999, ApJ, 522, 82

Knebe A., Kravtsov, A.V., Gottlöber, S., & Klypin A. 2000, MNRAS in press (astro-ph/9912257)

Kravtsov, A.V. 1999, Ph.D. Thesis, New Mexico State University

Kravtsov, A.V., Klypin, A., & Khokhlov, A.M. 1997, ApJS 111, 73

Kravtsov, A.V., Klypin, A., Bullock, J.S., & Primack, J.P. 1999, ApJ 502, 48

Kravtsov, A.V., & Klypin, A. 1999, ApJ 520, 437

Lokas, E.L., & Mamon, G. 2000, submitted to MNRAS, astro-ph/0002395

McGaugh, S. et al. 2000, in preparation

Moore, B. 1994, Nature 370, 629

Moore, B., Governato, F., Quinn, T., Stadel, J., Lake, G. 1998, ApJ 499, L5

Moore, B., Quinn, T., Governato, F., Stadel, J., Lake, G. 1999, MNRAS 310, 1147

Navarro, J.F., Frenk, C.S., & White, S.D.M. 1996, ApJ 462, 563

Navarro, J.F., Frenk, C.S., & White, S.D.M. 1997, ApJ 490, 493

Navarro, J.F., & Steinmetz, M. 2000, ApJ 528, 607

Navarro, J.F., & Swaters, R.A. 2000, in preparation

Swaters, R.A., Madore, B.F., Trehella, M. 2000, ApJ 531, L107

van den Bosch, F.C., Robertson, B.E., Dalcanton, J.J., de Blok W.J.G. 2000, AJ 119, 1579

van den Bosch, F.C. & Swaters, R.A., 2000, AJ,
submitted, astro-ph/0006048

Widrow, L. 2000, submitted to ApJ., astro-
ph/0003302